

Investigation of the electro-optic effect in high- Q 4H-SiC microresonators

RUIXUAN WANG,¹ JINGWEI LI¹, LUTONG CAI¹, AND QING LI^{*1}

¹*Department of Electrical and Computer Engineering, Carnegie Mellon University, Pittsburgh, PA 15213, USA*

**qingli2@andrew.cmu.edu*

Abstract: Silicon carbide (SiC) recently emerged as a promising photonic and quantum material owing to its unique material properties. Here, we carry out a first experimental investigation of the electro-optic effect in high-quality-factor 4H-SiC microresonators. Our findings, in particular the disappearance of the electric-optic response at AC frequencies above the megahertz level, point to a seeming lack of the fast Pockels effect in most of commercially available 4H-SiC wafers and suggest that the observed electro-optic tuning is likely to be induced by other mechanisms such as strain.

© 2022 Optical Society of America

Silicon carbide (SiC), a wide-bandgap compound semiconductor composed of silicon and carbide, is playing an increasingly important role in modern power electronics including electric-vehicle charging [1]. In addition, considerable research efforts have been devoted to studying its potential for photonic and quantum applications, resulting in the demonstration of low-loss SiC-on-insulator (SiCOI) integrated photonics platforms and the discovery of a variety of color centers with promising quantum properties [2, 3]. Among its many polytypes such as 3C, 4H and 6H, 4H-SiC gains the most attention from the industry as single-crystal 4H-SiC substrates up to six inches are already commercially available. Thanks to the continuously improved material quality, 4H-SiCOI has achieved a much lower propagation loss compared to other polytypes [4], which is a key enabling factor for applications such as low-power optical parametric oscillation [5] and broadband microcomb generation [6].

For integrated photonic circuits, one important functionality that underpins applications including optical signal modulation and switching is the electro-optic (EO) tuning [7]. That is, the application of an external electric field in the radio frequency or below leads to a change in the optical absorption and/or the refractive index of the hosting material. Two prominent examples are the plasma dispersion effect in silicon [8] and the Pockels effect in lithium niobate [9]. For the SiCOI integrated photonics platform, thus far only the EO effect in 3C-SiC has been experimentally demonstrated, which is based on the fast Pockels effect and hence capable of delivering GHz-level bandwidths [10, 11]. Theoretical calculations predict that 4H-SiC should have a similar Pockels effect [12], though to date no experimental evidence has been reported and it is unclear whether fast EO modulation/switching is attainable in 4H-SiC [13].

In this Letter, we carry out a first experimental investigation of the Pockels effect in 4H-SiC. For this purpose, low-loss microresonators are fabricated on on-axis (i.e., c -axis along z in Fig. 1(a)), semi-insulating 4H-SiCOI wafers [6]. One such example is provided in Fig. 1(b), where light from a tunable laser source is coupled to a racetrack resonator using on-chip waveguides and grating couplers [6]. To realize efficient EO tuning, electrodes are placed near the waveguide mode without introducing additional optical losses (Fig. 1(a)). Given the large resistivities from the 4H-SiC and surrounding oxide layers, there is no current flow between the signal and ground electrodes. (The resistance between the signal and ground pads is experimentally verified to be larger than 10 M Ω .) Instead, the EO effect is expected to be dominated by the field-induced change in the refractive index of SiC, which in turn shifts the cavity's resonance wavelength.

As illustrated by Fig. 1(c), we quantify the EO effect in SiC microresonators by fixing the input laser's wavelength at a proper bias and applying a sinusoidal electrical signal with varied amplitude and frequency. The EO-induced resonance wavelength shift ($\Delta\lambda_c$) is inferred from the amplitude modulation in the laser transmission, which has the same frequency as the electrical signal (see one example in Fig. 1(d)). In this regard, a high- Q resonance is beneficial given that the minimally detectable $\Delta\lambda_c$ is proportional to the cavity's linewidth.

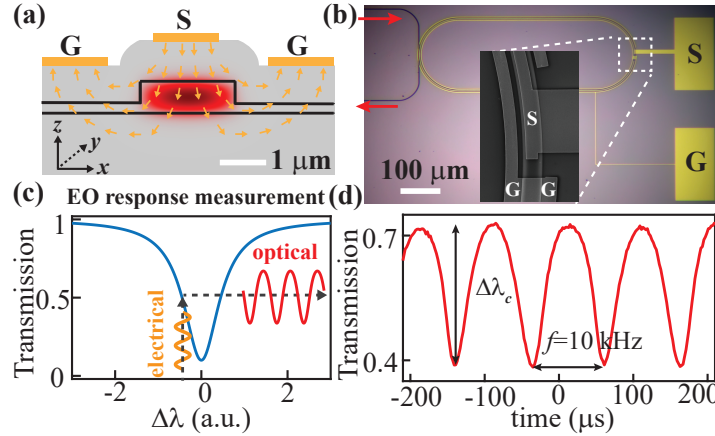


Fig. 1. (a) Cross-sectional view of a 4H-SiC rib waveguide with the signal and ground electrodes implemented near the waveguide mode (red colored). The 4H-SiC waveguide is surrounded by PECVD oxide. (b) Optical micrograph of a SiC racetrack resonator along with the electrical pads. The inset shows the scanning electron micrograph of the conjunction between the signal electrode on top of the waveguide and the connecting wire to the pad. (c) The electro-optic effect is quantified by measuring the optical transmission of a high- Q SiC microresonator in response to an applied electrical signal. (d) Exemplary transmission measured in a high- Q racetrack resonator with a sinusoidal electrical input at a frequency of 10 kHz and a peak-to-peak amplitude of 5 V. The corresponding resonance shift ($\Delta\lambda_c$) is inferred from the modulation amplitude.

In Fig. 2, measurement results for two racetrack resonators fabricated on a 4H-SiC wafer from ST Microelectronics (formerly known as Norstel AB and hereinafter referred to as "Norstel" for short) are provided. Both devices have an approximate waveguide width of 2500 nm, a nominal SiC thickness of 850 nm, and a pedestal layer of 250 nm. The bending radius of the racetrack resonator is chosen to be 100 μm (with circumference near 1.3 mm) to minimize the radiation loss. After ebeam lithography and dry etching, a 1-μm-thick PECVD oxide is deposited on top of the SiC microresonator, and electrodes made of Ti/Au layers are fabricated using the ebeam evaporation and liftoff process. To avoid the optical loss from the metal layer, the ground electrodes are placed 1 μm away from the sidewall of the SiC waveguides (Fig. 1(a)).

As can be seen from Fig. 2, optical resonances with intrinsic Q s up to 5 million are observed for the transverse-electric (TE, dominant electric field in the $x - y$ plane as indicated in Fig. 1(a)) and transverse-magnetic (TM, dominant electric field along the z axis as indicated in Fig. 1(a)) resonant modes in the 1550 nm wavelength band. These optical Q s are comparable to the state of the art [4, 5], which make our EO measurement extremely sensitive to even a small amount of resonance shift. In addition, by focusing on the amplitude modulation at the same frequency of the applied electrical signal, we can suppress the ubiquitous thermal noise, which causes random fluctuations (albeit small) in the bias point due to wavelength instabilities from both the microresonator and the input laser.

To understand the significant difference in the EO responses between the TE and TM

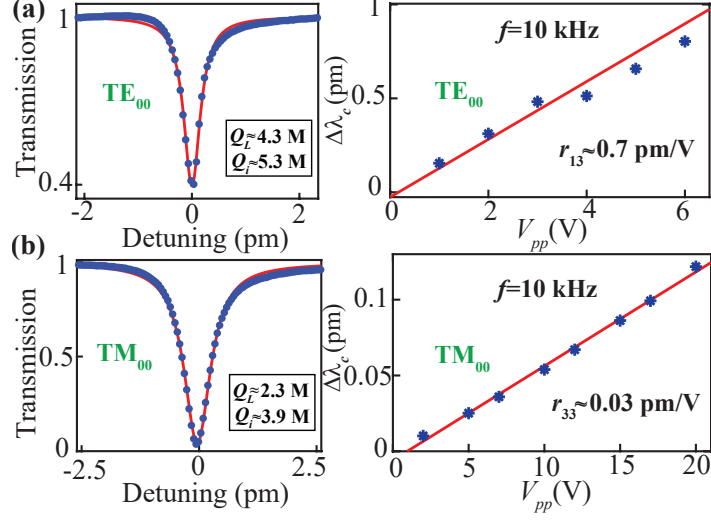


Fig. 2. Measured EO responses of the fundamental TE (TE_{00}) and TM (TM_{00}) modes in 4H-SiC (Norstel) racetrack resonators. The left figure in (a) and (b) plots the swept-wavelength transmission of the select high- Q resonance in the 1550 nm band, and the right figure shows the measured resonance wavelength shifts for varied peak-to-peak voltages (V_{pp}) of a sinusoidal electrical signal with a fixed frequency of 10 kHz.

polarizations and extract their corresponding EO coefficients, we utilize the fact that on-axis 4H-SiC wafers have a hexagonal crystal structure with an extraordinary refractive index (n_e) along the z axis and an ordinary refractive index (n_o) in the $x - y$ plane (see Fig. 1(a)). For the electrode configuration shown in Fig. 1(a), the dominant component of the electrical signal is along the z axis. A straightforward analysis based on the electro-optic tensor yields

$$\Delta\lambda_c(\text{TE}) = \frac{\lambda_0 n_o^2 \Gamma}{2} r_{13} \langle |E_z| \rangle, \quad (1)$$

$$\Delta\lambda_c(\text{TM}) = \frac{\lambda_0 n_e^2 \Gamma}{2} r_{33} \langle |E_z| \rangle, \quad (2)$$

where λ_0 is the resonance wavelength, Γ is the mode confinement factor ($\Gamma \approx 1$ for the waveguide modes studied here), r_{13} and r_{33} are the EO coefficients of 4H-SiC, and $\langle |E_z| \rangle$ is the spatially averaged electrical signal inside the SiC waveguide. By numerically simulating the electric field for a given voltage (see examples in Fig. 3), we extract r_{13} and r_{33} for the Norstel 4H-SiC to be around 0.7 pm/V and 0.03 pm/V, respectively.

In order to investigate the nature of the observed EO effect, we vary the frequency of the electrical signal for the TE mode in Fig. 2(a) with a fixed voltage ($V_{pp} = 2$ V), and normalize the measured EO response to that of $f = 10$ kHz. As shown in Fig. 3, the EO shift becomes significantly smaller at AC frequencies below 100 Hz, and nearly disappears at 1 Hz or below [11]. In fact, the EO shift at DC is still much smaller than 1 pm even with 100 V applied voltage. While surprising for the supposedly high-quality semi-insulating 4H-SiC wafers, this kind of frequency dependence can be explained by the significantly smaller resistivity of the 4H-SiC layer compared to that of the surrounding oxide layer. For example, the average resistivity of the Norstel 4H-SiC wafer used in this work is measured around $1.7 \times 10^9 \Omega \cdot \text{cm}$ [14], which is 7-8 orders lower than that of silicon dioxide. The two simulation examples for $f = 1$ Hz and $f = 10$ kHz shown in Fig. 3 suggest that the smaller EO response at low AC frequencies can be primarily attributed to the smaller electric field within the SiC waveguide and the likely degradation of

4H-SiC's resistivity with increased frequencies. Nevertheless, our simulation predicts that the impact of the limited resistivity from 4H-SiC should become negligible for high-enough AC frequencies. However, the experimental data in Fig. 3 has a fast roll off when the AC frequency is above 100 kHz, ruling out the fast Pockels effect as the underlying mechanism for the observed EO response and favoring other mechanisms such as strain [15].

The overall EO behavior, that the TE polarization has a much stronger EO response than TM and the disappearance of the EO effect at AC frequencies above the MHz level, has been consistently observed from other devices on the same Norstel chip. We also carried out similar nanofabrication and EO measurements for semi-insulating 4H-SiC wafers from II-VI and Cree [14], and observed similar results. The only major difference is in the EO response at the low frequency range, as the resistivities of 4H-SiC wafers of different grades and from different manufacturers can vary by orders of magnitude. However, all the SiC devices we tested exhibit diminishing EO responses above the MHz level, which is surprising given the non-centrosymmetric crystal structure of 4H-SiC and favorable theoretical predictions for its EO properties [12]. Further, we do observe second-harmonic generation (SHG) in all the 4H-SiC wafers tested in this work [16], which can be considered as an optical-frequency version of the EO effect. At this stage, we believe more experimental evidence will be needed to clarify the matter, in particular with respect to the potential of fast EO operations in 4H-SiC.

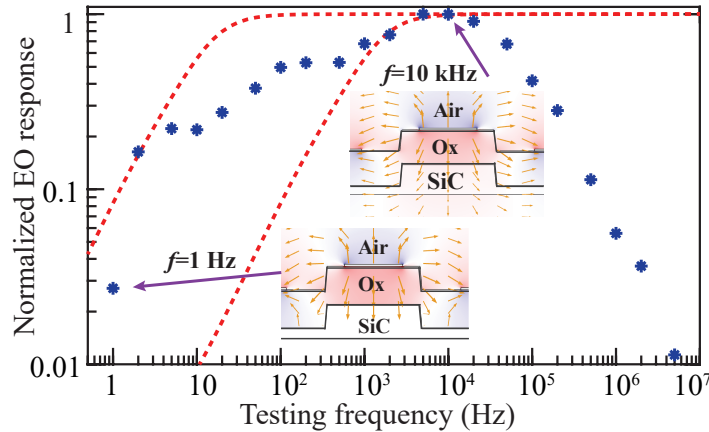


Fig. 3. The blue stars are the measured and normalized (using $f = 10$ kHz as the reference) electro-optic response of the TE₀₀ mode in Fig. 2(a) at varied testing frequencies for a fixed $V_{pp} = 2$ V. The two dashed red lines are the simulated EO responses, with the left (right) corresponding to the SiC's resistivity of 10^{10} (10^8) $\Omega \cdot \text{cm}$. The two insets plot the electric field at $f = 1$ Hz and $f = 10$ kHz, assuming a SiC resistivity of $1.7 \times 10^9 \Omega \cdot \text{cm}$.

To summarize, we performed a preliminary experimental investigation of the electro-optic effect in high- Q 4H-SiC microresonators for the first time. The observed EO response is much stronger for the TE-polarized optical modes than the TM polarization. In addition, the EO effect in 4H-SiC can only operate up to the sub-MHz range, suggesting the surprising absence of the fast Pockels effect and the need of more investigations to further understand the root cause.

Funding. This work was supported by DARPA (D19AP00033) and NSF (2127499).

Acknowledgments. The authors would like to thank discussions with Prof. James Bain and the equipment support from Prof. Xu Zhang's group at ECE. J. Li also acknowledges the support of Axel Berny Graduate Fellowship from CMU.

Disclosures. The authors declare no conflicts of interest.

Data Availability. Data underlying the results presented in this paper are not publicly available at this time but may be obtained from the authors upon reasonable request.

References

1. T. Kimoto, "Material science and device physics in SiC technology for high-voltage power devices," *Jpn. J. Appl. Phys.* **54** (2015).
2. C. P. Anderson, A. Bourassa, K. C. Miao, G. Wolfowicz, P. J. Mintun, A. L. Crook, H. Abe, J. U. Hassan, N. T. Son, T. Ohshima, and D. D. Awschalom, "Electrical and optical control of single spins integrated in scalable semiconductor devices," *Science* **366**, 1225–1230 (2019).
3. D. M. Lukin, M. A. Guidry, and J. Vučković, "Integrated quantum photonics with silicon carbide: challenges and prospects," *PRX Quantum* **1**, 020102 (2020).
4. Y. Zheng, M. Pu, A. Yi, X. Ou, and H. Ou, "4H-SiC microring resonators for nonlinear integrated photonics," *Opt. Lett.* **44**, 5784 (2019).
5. M. A. Guidry, D. M. Lukin, K. Y. Yang, R. Trivedi, and J. Vučković, "Quantum optics of soliton microcombs," *Nat. Photonics* **16**, 52–58 (2022).
6. L. Cai, J. Li, R. Wang, and Q. Li, "Octave-spanning microcomb generation in 4H-silicon-carbide-on-insulator photonics platform," *Photonics Res.* **10**, 870–876 (2022).
7. R. Soref and B. Bennett, "Electrooptical effects in silicon," *IEEE J. Quantum Electron.* **23**, 123–129 (1987).
8. Q. Xu, B. Schmidt, S. Pradhan, and M. Lipson, "Micrometre-scale silicon electro-optic modulator," *Nature* **435**, 325–327 (2005).
9. C. Wang, M. Zhang, X. Chen, M. Bertrand, A. Shams-Ansari, S. Chandrasekhar, P. Winzer, and M. Lončar, "Integrated lithium niobate electro-optic modulators operating at CMOS-compatible voltages," *Nature* **562**, 101–104 (2018).
10. T. Fan, X. Wu, S. R. M. Vangapandu, A. H. Hosseinnia, A. A. Eftekhari, and A. Adibi, "Racetrack microresonator based electro-optic phase shifters on a 3C silicon-carbide-on-insulator platform," *Opt. Lett.* **46**, 2135–2138 (2021).
11. K. Powell, L. Li, A. Shams-Ansari, J. Wang, D. Meng, N. Sinclair, J. Deng, M. Lončar, and X. Yi, "Integrated silicon carbide electro-optic modulator," *Nat. Commun.* **13**, 1851 (2022).
12. I. J. Wu and G. Y. Guo, "Second-harmonic generation and linear electro-optical coefficients of SiC polytypes and nanotubes," *Phys. Rev. B* **78**, 035447 (2008).
13. A. Yi, C. Wang, L. Zhou, Y. Zhu, S. Zhang, T. You, J. Zhang, and X. Ou, "Silicon carbide for integrated photonics," *Appl. Phys. Rev.* **9**, 031302 (2022).
14. J. Li, R. Wang, L. Cai, and Q. Li, "Measurement of the Kerr nonlinear refractive index and its variation among 4H-SiC wafers," (2022). [ArXiv:2211.09220](https://arxiv.org/abs/2211.09220).
15. R. S. Jacobsen, K. N. Andersen, P. I. Borel, J. Fage-Pedersen, L. H. Frandsen, O. Hansen, M. Kristensen, A. V. Lavrinenko, G. Moulin, H. Ou, C. Peucheret, B. Zsigri, and A. Bjarklev, "Strained silicon as a new electro-optic material," *Nature* **441**, 199–202 (2006).
16. B.-S. Song, T. Asano, S. Jeon, H. Kim, C. Chen, D. D. Kang, and S. Noda, "Ultrahigh-Q photonic crystal nanocavities based on 4H silicon carbide," *Optica* **6**, 991 (2019).